# Optimization of anchor trench design for solar evaporation ponds

Thiel, R.
*Thiel Engineering, Oregon House, CA, USA, Richard@rthiel.com*

Keywords: anchor trench, wind forces, pullout, exposed geomembrane

ABSTRACT: Ponds with exposed geomembranes on their sideslopes will be susceptible to wind forces, which must be resisted by properly designed anchorages at the slope crest. The most common anchorage is an earth-filled anchor trench. This paper describes improved methods used to optimize the anchor trench design to conserve material and minimize earthwork for a V-shaped anchor trench.

## 1 INTRODUCTION

A series of 10 hectare (ha) geomembrane-lined ponds were planned to evaporate potash salt. The ponds were designed with 1(V):2(H) side slopes ranging in height from 2 to 12 m. The side slopes would have the geomembrane exposed.

One of the value-engineering goals was to design the anchor trenches to involve minimal construction effort while resisting pullout due to possible wind forces. The estimated wind forces were calculated using the Giroud et al. (1995) method for a 145 km/hr wind speed.

Most simple design models that could be used for determining the required dimension of the anchor trench to resist wind pullout forces would result in overly-conservative large dimensions because they ignore corner resistance forces. Since there would be over 16 km of anchor trench on the project, there was a desire to optimize the sizing of the anchor trench so as to avoid overbuilding it from a cost point of view.

Existing design methodologies were reviewed, and recommendations were developed in this project to evaluate economical anchor trench sizes for V-shaped trenches. As a result of the methodology used in this project, a cost-effective schedule of V-shaped anchor trenches was prepared that varied the required size of the V-trench with the height of the slope. The design parameters for the anchor trench, shown in Figure 1, are as follows: $D$ (anchor trench depth); $B$ (trench width); $L$ (runout length); $H$ (soil depth above runout); $\gamma$ (soil unit weight); $\delta_1$ and $\delta_2$ (soil/geomembrane friction angle on upper and lower interfaces, respectively); $\psi_1$, $\psi_2$, and $\psi_3$ (geomembrane angles); $\beta$ (pond slope); $T$ (geomembrane tension due to wind); and $\theta$ (tension pullout angle).

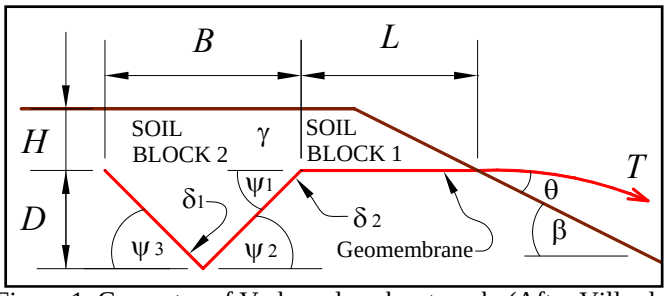


Figure 1. Geometry of V-shaped anchor trench. (After Villard and Chareyre, 2004)

## 2 ANCHOR TRENCH MODELS

The fundamental resistances to tension pullout are derived from shear resistance between the geomembrane, and the soils above and below the geomembrane. Most textbook methods for evaluating anchor trench pullout only consider the shear resistance along the planar surfaces of the anchor trench (e.g. the trench walls), and they assume "frictionless rollers" at the corners. The most common approaches as suggested by Koerner (1998) and Qian et al. (2002) were perceived as providing inadequate consideration for pullout resistance around corners in the anchor trench. There is no reason to neglect slipping resistance around corners, however, and the approach described in this paper provides a method to account for that. It is intuitive that the more corners there are in an anchor trench, the more difficult it will be to pull out the membrane. Thus, to optimize anchor trench design on large projects the corner resistance should be accounted for.

The most comprehensive anchor trench design methodology presented in the literature was found to be Villard and Chareyre (2004). Villard and Chareyre (2004) used a combination of analytical reasoning, finite element modeling, and laboratory testing to recommend a design approach for L- and V-shaped anchor trenches. The analytical methodology proposed by Villard and Chareyre (2004) was consider by the current author to be far superior to any other methodologies previously proposed, and was used as the basis for this case study.

There are two methods proposed by Villard and Chareyre (2004) to consider slip resistance around a corner. The first method is based on the 18th-century Euler-Eytelwein equation for friction of a belt slipping around a curved cylinder. This equation, illustrated in Figure 2, is commonly used in the conveyor belt industry and in the electrical and welding industries where wire is pulled through conduits.

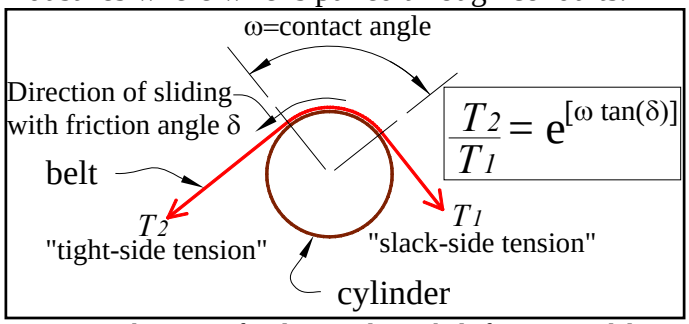

Figure 2. Schematic of Euler-Eytelwein belt-friction model.

Predictions of the belt-to-cylinder friction force using this equation have been recognized to over- and under-estimate actual tension ratios, but have generally proven to be acceptable in engineering applications, with errors in the range of 15% [Padilla et al. (2003) and Belofsky (1973)]. The simplifying errors of the equation have generally been offset by errors in the assumed friction values.

Villard and Chareyre (2004) noted that the Euler-Eytelwein equation correlated well with experimental and finite-element predictions for anchor trench pullout resistance in stiff soils that have small deformations at the anchor trench corners. The Euler-Eytelwein equation appears to overpredict pullout resistance, however, compared with experimental and finite-element results for loose sandy soils that have relatively large deformations at the anchor trench corners. The second analytical method proposed by Villard and Chareyre (2004) to account for corner resistance was for "loose sands", and was based on limit equilibrium statics for a rigid body. Their "loose-sand" model, which is not reviewed in detail in this paper for lack of space, is questionable, however, because it frequently indicates unrealistic trends of a decreasing tension ratio with an increasing corner angle, and unrealistic tension ratios of less than one. They conclude that a minimum conservative tension ratio for $T_2/T_1$ is obtained by setting the normal force perpendicular to the tight-side tension, with a minimum allowable tension-ratio equal to unity. If the ratio were indeed equal to unity, then there would be zero friction loss around the corner, and statics would dictate that the normal force generated against the soil corner would bisect the angle between the two tension forces, contrary to their assumption that it would be perpendicular to the tight-side tension.

The current author would suggest that for any project where an optimal anchorage design is desired, the backfill soil should be well compacted. For stiff/dense well-compacted soils the Euler-Eytelwein equation is deemed to be an appropriate model to estimate the sliding resistance around a corner, and will be used in the remainder of this paper. Further refinements of the Euler-Eytelwein equation could be considered, and have been proposed in other industries (e.g. Belofsky, 1973; Padilla et al. 2003). These refinements may be of secondary importance compared to the level of approximation used in the estimation of the friction angle between the geomembrane and the adjacent soils.

## 3 FORCE DIAGRAMS AND EQUATIONS

The free-body diagrams shown in Figures 3-5 are used to derive the analytical model for a V-shaped anchor trench pullout resistance. This approach was also performed by Villard and Chareyre (2004), but the consideration of all of the forces is considered more complete in the current paper.

A free-body diagram (FBD) of the forces acting on the geomembrane in the anchor trench is shown in Figure 3. The goal is to calculate the pullout resistance, $T_1$, of the geomembrane. This is accomplished by analyzing from the back of the anchor trench to the front. The following nomenclature is used with the free-body diagrams and force polygons:

- $W_i$ = weight of overlying soil
- $S_i = N_i \tan\delta_i$ = shear force along geomembrane interface at location $i$
- $R_i$ = resultant force at a corner
- $N_i$ = normal force along a geomembrane side
- $T_i$ = tension in a geomembrane segment

An expression for the tension $T_3$ in the tail end of the anchor trench can be written in terms of $N_3$ as:

$$T'_3 = S_{31} + S_{32} = N_3(\tan\delta_1 + \tan\delta_2) \quad (1)$$

It is tempting to consider that $N_3$ can be directly calculated from the weight of soil block no. 2, and that $N_3 = N_2$. If that were the case, then the remainder of the calculations would be fairly straightforward. This is an incorrect assumption that is made in other over-simplified methods presented in the literature. A more rigorous evaluation of the static equilibrium, as described in this paper, reveals a more complex relationship. The validity of the me-

thod described herein is validated by finite-element modeling presented by Villard and Chareyre (2004).

From the Euler-Eytelwein equation presented in Figure 2, we have the corner force relationship:

$$T_3 = T'_3 e^{(\psi_2+\psi_3)\tan\delta_1} \quad (2)$$

Defining $K_3 = e^{(\psi_2+\psi_3)\tan\delta_1}$ we have

$$T_3 = K_3 T'_3 \quad (3)$$

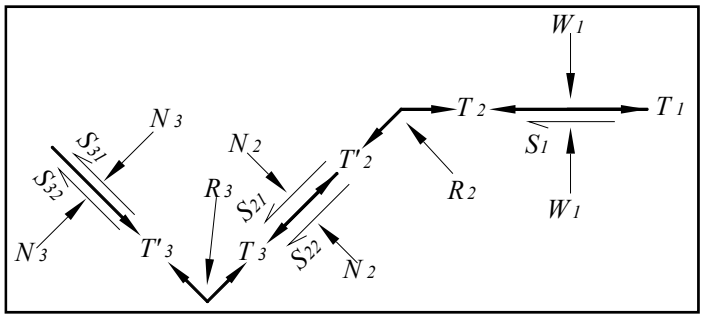


Figure 3. Free-body diagram of forces acting on individual segments of the anchored geomembrane.

Figure 4 presents a free-body diagram (FBD) and a force polygon of the bottom trench corner.

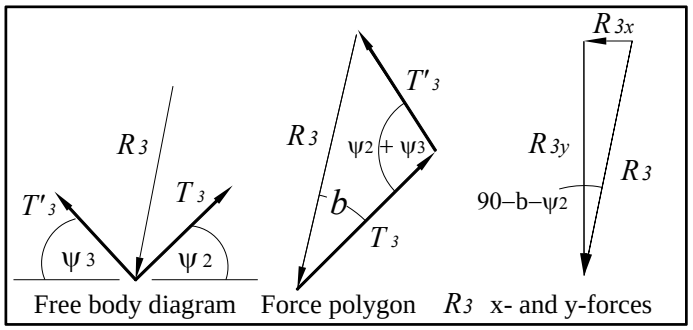


Figure 4. FBD and force polygon at lower corner of anchorage.

The resultant force $R_3$ can be solved using the law of cosines as:

$$R_3 = T'_3 C_3 \quad (4)$$

Where:

$$C_3 = [1 + K_3^2 - 2K_3\cos(\psi_2 + \psi_3)]^{0.5} \quad (5)$$

The angle $b$ can be solved using the law of sines as:

$$b = \sin^{-1}\left[\sin(\psi_2 + \psi_3)/C_3\right] \quad (6)$$

The x- and y- directions for $R_3$ can now be resolved as:

$$R_{3x} = T'_3 C_3 \sin(90\text{-}b\text{-}\psi_2) \quad (7)$$

$$R_{3y} = T'_3 C_3 \cos(90\text{-}b\text{-}\psi_2) \quad (8)$$

Referring to Figure 5, and summing forces in the x and y directions yields the following:

$$N_2\sin\psi_2 = S_{21}\cos\psi_2 + S_{31}\cos\psi_3 + N_3\sin\psi_3 + R_{3x} \quad (9)$$

$$N_2\cos\psi_2 + N_3\cos\psi_3 + R_{3y} + S_{21}\sin\psi_2 = W_2 + S_{31}\sin\psi_3 \quad (10)$$

Rearranging Eqn (9) yields the following (all the steps are not shown to save space):

$$N_2 = T'_3 C_5 \quad (11)$$

Where:

$$C_5 = \left(\frac{1}{\sin\psi_2 - \tan\delta_1\cos\psi_2}\right)\left[\left(\frac{\tan\delta_1\cos\psi_3}{\tan\delta_1+\tan\delta_2}\right) + \left(\frac{\sin\psi_3}{\tan\delta_1+\tan\delta_2}\right) + C_3\sin(90 - b - \psi_2)\right] \quad (12)$$

Rearranging Eqn (10) yields the following:

$$T'_3 = W_2 C_6 \quad (13)$$

Where $W_2$ can easily be calculated from the unit weight and geometry, and where:

$$C_6 = \left[C_5\cos\psi_2 + \frac{\cos\psi_3}{(\tan\delta_1+\tan\delta_2)} + C_3\cos(90 - b - \psi_2) + C_5\tan\delta_1\sin\psi_2 - \left(\frac{\tan\delta_1\sin\psi_3}{\tan\delta_1+\tan\delta_2}\right)\right]^{-1} \quad (14)$$

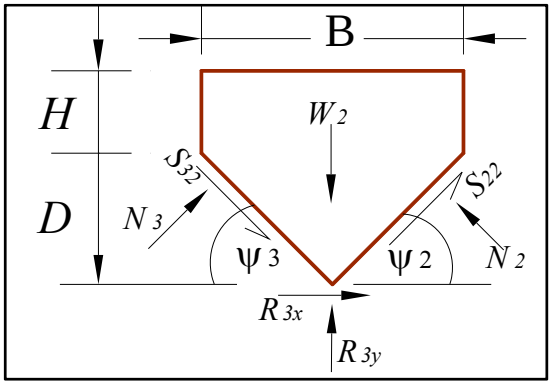


Figure 5. Free-body diagram of soil block 2.

Having solved for $T'_3$ in Eqn (13) allows for calculation of $T_3$ and $N_2$ (and therefore $S_{21}$ and $S_{22}$, as well) using Eqns (2) and (11), respectively. This then allows calculation of $T'_2$ as:

$$T'_2 = T_3 + S_{21} + S_{22} \quad (15)$$

Using Eqns (2) and (3) in a similar fashion for corner no. 2 as was used for corner no. 3, and defining $K_2 = e^{(\psi_1)\tan\delta_2}$ we obtain

$$T_2 = K_2 T'_2 \quad (16)$$

This now allows for the calculation of $T_1$ as:

$$T_1 = T_2 + S_1 = T_2 + W_1\tan\delta_2 \quad (17)$$

The weight of soil block no. 1, $W_1$, is easily calculated using the soil unit weight and geometry. Note that soil block no. 1 is assumed to slide with the geomembrane. If $T_1$ is pulling at an angle that would cause a corner resistance with the outer edge of the slope, then one additional calculation, similar in nature to Eqns (3) or (16), could be performed.

Note that the value for $R_2$ could be determined using the procedure shown in Figure 4. Although it is not needed for the solution of $T_1$, it is useful to compute so that a check on the stability of the soil wedge under the anchor trench at the crest of the

slope can be performed. Further explanation of this issue is beyond the scope of this short paper.

## 4 CASE HISTORY RESULTS

For this case history, the only variable was the anchor trench depth, $D$ (which also controls $B$, the trench width), which would be optimized for the various slope and wind-pullout conditions. The other parameters were as follows: $L$ = 0.91m; $H$ = 0.15m; $\gamma$ = 17.28 kN/m$^3$; $\delta_1$=$\delta_2$= 20°; $\psi_1$= $\psi_2$= $\psi_3$ = 45°; $\beta$ = 22°; $T$ = values shown in Table 1 calculated using the Giroud et al. (1995) method for different slope conditions. The tension pullout angle, $\theta$, was assumed equal to $\beta$ in all conditions, thus offering no corner resistance at that location. The results for the various slope heights with a factor of safety (FS) equal to unity are presented in Table 1.

Table 1. Design Results for Case History

| Slope height (m) | Estimated geomembrane tension $T$ (kN/m) | Calculated value of $D$ req'd for V-trench by method in this paper (m) | Calculated value of $D$ req'd by method of Villard and Chareyre (2004) (m) |
|---|---|---|---|
| 2.44 | 7.25 | 0.497 | 0.504 |
| 4.57 | 10.7 | 0.641 | 0.645 |
| 11.6 | 18.6 | 0.896 | 0.900 |

It is interesting to note that the value calculated for $N_2$ in this example is approximately 3 times the value of $N_3$ for all slope heights. Even though the geometry of the V-trench is symmetric relative to these two forces, the static equilibrium results in substantially different normal forces on the two flanks of the V. This result is much different than other simplified methods presented in the literature.

## 5 CONCLUSIONS AND DISCUSSION

The objective of this paper is aimed towards optimizing the anchor trench design on projects with exposed geomembranes where efficiency in anchor trench construction is desired. The analytic method proposed by Villard and Chareyre (2004) is considered by the current author to have been the best and most comprehensive evaluation of anchor trench design previously developed. Although some changes were made by the current author to reflect his interpretation of the appropriate equilibrium conditions, the new results compare very favorably with the results using the original Villard and Chareyre (2004) method.

Given the premise that optimized anchor trench geometry is desired for exposed wind-resistant applications, one main conclusion is that the anchor trench subgrade and backfill materials should be well compacted as a basic requirement for an optimized design.

For critical applications, a factor-of-safety is recommended, whose value should be commensurate with the level of confidence in understanding the interface shear strength parameters.

It is interesting to compare the effect of different V-trench angles. In general, a steeper angle on the slope side of the trench will provide more resistance. Figure 6 indicates that a 60°-30° V-trench can be slightly shallower and use about the same amount of geomembrane material to provide the same anchorage resistance as a 45°-45° V-trench. It should be noted that a steeper angle on the front side of the trench will put more pressure on the soil wedge under the leading edge of the anchor trench, and the stability of that wedge should be checked.

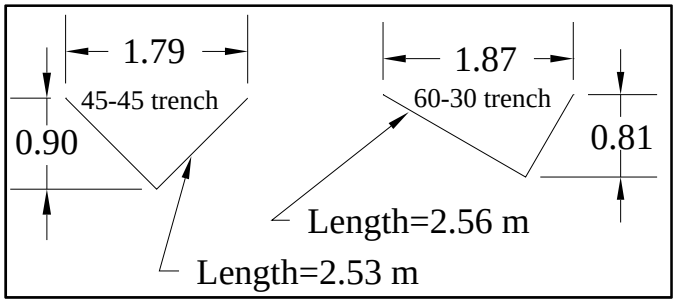


Figure 6. Comparison of two V-trench geometries that provide equal pullout resistance.

The approach described in this paper can be extended to other trench geometries, such an L-shaped trench, but additional considerations for lateral earth pressures on vertical or near-vertical surfaces would need to be evaluated.

More work is needed to understand how different soil types, consistencies, and stiffnesses affect the anchor trench pullout response at corners.

## REFERENCES


Belofsky, H. 1973. On the theory of power transmission by a flat, elastic belt. *Wear*. Elsevier Sequoia, S.A., Lausanne. V75, pp. 73-84.

Giroud, J.P., Pelte, T. and Bathurst, R.J. 1995. Uplift of geomembranes by wind. *Geosynthetics International*. V2N6, pp. 897-952.

Koerner, R.M. 1998. *Designing with geosynthetics.* 4th ed. Prentice-Hall, NJ., pp. 487-494.

Padilla, T.M., Quinn, T.P., Munoz, D.R., and Rorrer, R.A.L. 2003. A mathematical model of wire feeding mechanisms in GMAW. *Welding Journal*. American Welding Society. May, 2003, Vol. 5(5), pp. 100s-109s.

Qian, X., Koerner, R.M, and Gray, D. 2002. *Geotechnical aspects of landfill design and construction.* Prentice-Hall, NJ., 717 pp.

Villard, P. and Chareyre, B. 2004. Design methods for geosynthetic anchor trenches on the basis of true scale experiments and discrete element modelling. *Canadian Geotechnical Journal.* V41, pp. 1193-1205.

Ponds with exposed geomembranes on their sideslopes are susceptible to wind forces, which must be resisted by properly designed anchorages at the slope crest. The most common anchorage is an earth-filled anchor trench. This article describes improved methods used to optimize the anchor trench design to conserve material and minimize earthwork for a V-shaped anchor trench. Discover the world's research. 19+ million members.Â  The most recent available methods for the design of anchor trenches are provided by Villard and Chareyre (2004) and Thiel (2010). Beyond all these aspects, it should be noted all the issues considered previously should be carefully analyzed (on a case by case basis) while designing a safety piggy-back system. Keywords: Solar Pond; Solar Evaporation; Carnallite Production; Phase Chemistry. 1. Introduction. Solar ponds are simple pools of saltwater where it acts as a large scale solar thermal energy collector [1] or it is used for minerals extraction such as the production of concentrated brines and salt deposits [2-4]. Solar ponds operated as thermal energy collector are used in various applications, such as process heating, desalination, re-frigeration, drying and solar power generation.Â  very sensitive to optimum design and more research efforts need to be conducted to fully understand the complex behavior and trends. Ð‡ The model also assumes that evaporation of all brines is correctly represented however its accuracy is not well examined. When designing evaporation ponds, it is best if a number of smaller ponds are constructed and connected by a pipeline. Smaller ponds are easy to manage especially in windy conditions where wave action can damage the levees requiring costly maintenance. Suitable site selection is very.Â  [3] suggested the use of evaporation ratio of 0.7 for multiplying calculated solar evaporation rate to incorporate the effect of salinity. They also suggested that pond depths ranging from 25 to 45 cm are optimal for maximizing the rate of evaporation. Very shallow evaporation ponds are subject to drying and cracking of the liners. An ideal evaporation pond must be able to accept reject brine at all times under all conditions.